Optics Letters

Direct measurements of forces induced by Bloch surface waves in a one-dimensional photonic crystal

Daniil A. Shilkin, Evgeny V. Lyubin, Irina V. Soboleva, and Andrey A. Fedyanin*

Faculty of Physics, Lomonosov Moscow State University, Moscow 119991, Russia
**Corresponding author: fedyanin@nanolab.phys.msu.ru*

Received 24 August 2015; revised 25 September 2015; accepted 28 September 2015; posted 29 September 2015 (Doc. ID 248492); published 19 October 2015

An experimental study of the interaction between a single dielectric microparticle and the evanescent field of the Bloch surface wave in a one-dimensional (1D) photonic crystal is reported. The Bloch surface wave-induced forces on a 1 μm polystyrene sphere were measured by photonic force microscopy. The results demonstrate the potential of 1D photonic crystals for the optical manipulation of microparticles and suggest a novel approach for utilizing light in lab-on-a-chip devices.

OCIS codes: (230.5298) Photonic crystals; (240.6690) Surface waves; (350.4855) Optical tweezers or optical manipulation.

http://dx.doi.org/10.1364/OL.40.004883

Optical radiation forces have been widely used in nano- and microparticle manipulation since the optical tweezers technique was developed in 1986 [1]. Optical tweezers are easy to use, noncontact, and noninvasive. Partly for these reasons, they have found numerous applications in studies of single living cells [2–4] and biological molecules [5–7], and in precise measurements of colloidal interactions [8–10]. In recent years, the potential of optical manipulation in microfluidic lab-on-a-chip devices has become increasingly attractive [11–13]. The evanescent fields generated by total internal reflection and surface plasmon polaritons have been proposed for integrating optical tweezers into planar lab-on-a-chip designs [14,15]. The forces acting on dielectric microparticles in these fields have been directly measured [16,17]. Optical trapping and transport of particles by optical waveguides and plasmonic structures have been experimentally demonstrated [18–21]. The use of surface plasmon resonance in metals has been shown to enhance the local electromagnetic field and optically induced forces, but these effects are always accompanied by local heating, which is undesirable in most biological applications.

Bloch surface waves (BSWs) are propagation modes in photonic crystals that are confined to the surface in a manner that is similar to that of surface plasmon polaritons. The excitation of BSWs in a one-dimensional (1D) photonic crystal was first observed in the 1970s [22]. After the prism-coupled excitation of BSWs was experimentally demonstrated [23], most studies have focused on sensing applications [24–26]. Discussion of the other effects related to BSWs had almost ceased until they were suggested as a novel basis for two-dimensional integrated optics a few years ago. The refraction and reflection of BSWs [27], and their focusing using a flat lens [28] and guiding with a ridge [29], have been experimentally demonstrated. The BSW-induced enhancement of the Goos–Hänchen effect has also been observed [30].

In this Letter, BSWs providing large local field enhancements in all-dielectric structures are considered as a novel tool for the optical manipulation of microparticles. The momentum of the BSW propagating in a 1D photonic crystal is experimentally demonstrated to be transferred to a dielectric microparticle located in the BSW evanescent field. The BSW-induced forces acting on the particle are measured by photonic force microscopy (PFM).

PFM is based on the analysis of particle displacements in an optical tweezers trap to measure the external forces acting on the particle [31,32]. In optical tweezers, a particle that is shifted from the trap center experiences the restoring force, which is proportional to the displacement in the case of small shifts [33]. The proportionality coefficient, known as the trap stiffness, is commonly determined through thermal motion analysis [34]. If some external force acts on the trapped particle, its equilibrium position changes in such a way that the resulting force becomes zero. When the trap stiffness is known, the external force is determined through particle displacement measurements, which can be performed with great accuracy [35].

In our experiment, a particle is trapped in optical tweezers in the vicinity of a 1D photonic crystal (see Fig. 1), and its displacement is measured when the BSW is excited.

The experimental setup consists of three main parts: the sample, the BSW excitation scheme, and the photonic force microscope. The sample is a 10^{-8} vol. × % water suspension of 1 μm polystyrene microspheres enclosed by a cover glass (refractive index of 1.52 and thickness of 140 μm) on one side and a 1D photonic-crystal (PC) on the other. The surfactant sodium dodecyl sulfate (SDS) is added to the suspension (concentration of 10 mM) to prevent adhesion of the particles. The

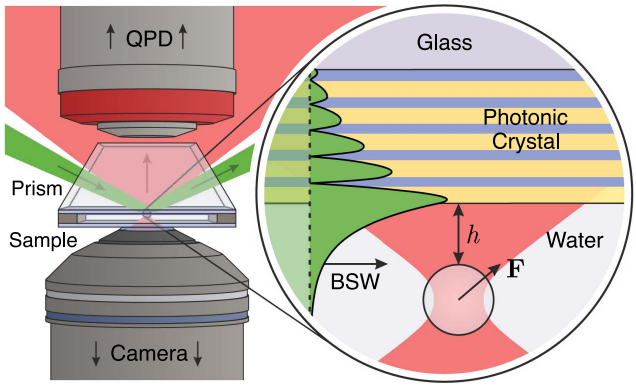

Fig. 1. Experimental schematic. A particle is trapped in optical tweezers (red) in the vicinity of a 1D photonic crystal, and its displacement is measured when BSW radiation (green) is turned on. In the inset, a magnified view is presented, and the BSW electric field distribution is indicated in green. QPD, quadrant photodiode; BSW, Bloch surface wave.

PC consists of five pairs of ZrO_2/SiO_2 quarter-wavelength layers deposited on a glass substrate. The PC band gap spectral position of 1200 nm was determined by transmittance spectroscopy. The spectroscopic ellipsometry was used to determine the thicknesses of each of the layers for further calculations.

The slightly focused *s*-polarized radiation of a CW frequency-doubled Nd-YAG laser (wavelength of 532 nm and power of 50 mW) illuminating the PC through a 55° glass prism (refractive index of 1.66) is coupled to the BSW at the PC/water interface using the attenuated total internal reflection configuration. Microscope immersion oil is used to ensure optical contact between the prism and the photonic crystal sample. The angular divergence of the radiation is approximately 0.4°, which provides a laser intensity in the sample of 1.6 kW/cm^2. The tighter focusing allows not only higher intensity to be achieved, but also leads to a higher divergence, which is undesirable because of the small width of the BSW resonance. The *p*-polarized radiation provides no BSW excitation at the sample and is used as a reference. The illuminating arm is mounted on a rotation stage for fine control over the angle of incidence.

The optical trap is formed by the radiation of a single-mode diode laser (wavelength of 975 nm) focused in the sample by a water-immersion objective with a NA of 1.2. A piezoelectric stage controls the focal waist position relative to the PC surface with nanometer accuracy. The image of the objective field of view is registered by a CMOS camera. The trapped particle position is determined by a quadrant photodiode (QPD) that detects the trapping beam radiation that is scattered at the particle. Thermal motion analysis is used to obtain the actual particle displacements [34].

One of the main difficulties associated with PFM measurements is correctly determining the distance between the particle and the surface. First, the surfactant SDS added to the suspension hinders beads moving near the PC surface. Second, there is a reflected beam, which interferes with the incident beam and influences the trap potential [36]. Consequently, the equilibrium position of the trapped bead is not directly determined by the position of the trapping laser waist and should be calibrated separately. The technique applied in this Letter is based on analyzing the variation in the hydrodynamic drag coefficients versus the trapping beam waist position [35].

During the measurements, the equilibrium position of the trapped particle relative to the PC surface is fixed by means of feedback control [37]. The histograms of the particle displacement probabilities in the presence and absence of the BSW, $P_{BSW}(x, z)$ and $P_0(x, z)$, are detected. The additional potential U_{BSW} resulting from the presence of the BSW field is obtained from $P(x, z) \propto \exp(-U(x, z)/k_B T)$, where k_B is the Boltzmann constant and T is the temperature. The BSW-induced force is determined as $\mathbf{F} = -\nabla U_{BSW}$.

The angular reflectance spectra of the sample illuminated with *s*- and *p*-polarized laser radiation at 532 nm are shown in Fig. 2(a). To obtain these spectra, the laser beam was not focused, and its angular divergence was less than 0.04°. Because the BSW in the samples appears only at the *s*-polarized illumination, the *p*-spectrum is shown as a reference. The dip in the spectrum for *s*-polarized radiation is related to the BSW excitation resonance. Numerical spectra shown as curves were calculated with the transfer matrix technique using the refractive indices, and layer thicknesses were obtained independently by ellipsometry and effective absorption coefficients of 2×10^{-5} for all of the materials. The BSW excitation leads to electromagnetic field localization close to the surface and its exponential decay into both water and the PC. The calculated field distribution over the PC layers at the BSW resonance is shown in Fig. 2(b).

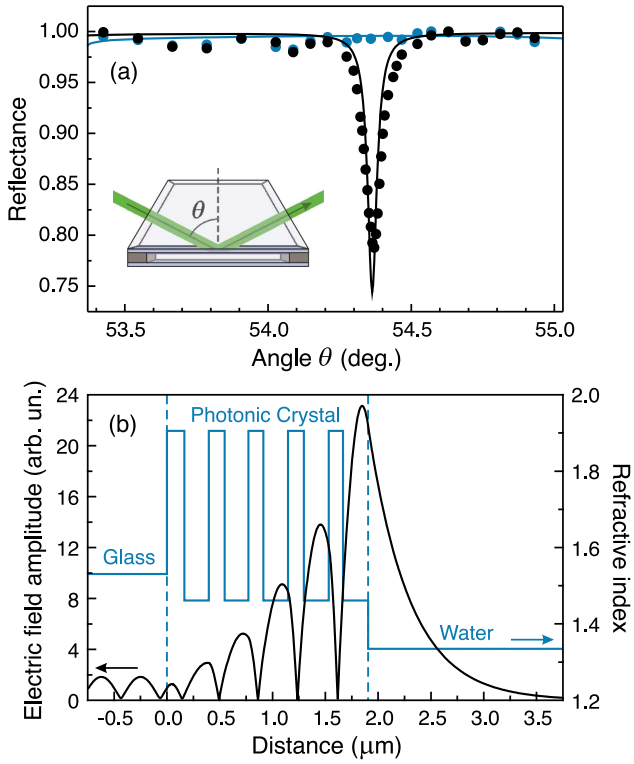

Fig. 2. (a) Experimental (dots) and calculated (solid) angular reflectance spectra of the PC sample in the Kretschmann configuration for *s*- (black) and *p*- (blue) polarized unfocused incident light. (b) Distribution of the refractive indices (blue) and calculated electric field amplitude at the BSW resonance (black) over the PC layers. The field is shown in units of the amplitude of the excitation radiation.

Optically induced forces on transparent particles are commonly considered as the sum of the scattering and gradient components. The BSW-induced scattering force can be observed in the directional motion of a particle located near the PC surface along the BSW propagation direction. A time-sequenced set of microimages demonstrating the particle propulsion in the BSW evanescent field is shown in Fig. 3. The particle is initially brought to the PC surface by the optical tweezers. After the trapping beam is shuttered, the bead motion is primarily determined by the BSW radiation forces. The bead is pulled by the BSW gradient force to the PC surface and propelled by the BSW scattering force. The latter can be estimated from the average bead drift velocity of $v = 7$ μm/s using Stokes' law $F = \gamma(h)v$, where the hydrodynamic drag coefficient γ is a function of the distance between the surface and the bead [38]. If one assumes the surface/particle gap to be 100 nm, a force value of 150 fN is obtained.

The PFM results are presented in Fig. 4. Figure 4(a) shows the angular dependences of the PC reflectance and a BSW radiation force at the PC/particle gap of approximately 300 nm. The maximum force value is obtained at the BSW excitation resonance. The width of the force dependence peak is similar to the width of the reflection spectrum dip and is approximately 0.4°, which is close to the angular divergence of the exciting radiation.

Figure 4(b) presents the coordinate projections of the BSW-induced force as a function of the distance between the bead and PC surface. The dependence is measured near the BSW excitation resonance angle. At large distances, the force decays exponentially with the intensity of the BSW. However, at PC/particle gaps of less than 150 nm there is a surprising force diminution.

To determine whether this effect is due to BSW field perturbation, we have carried out three-dimensional numerical FDTD simulations. In Fig. 5(a), the BSW electric field amplitude at the presence of a 1 μm spherical particle is shown. The BSW propagates from the left to the right. The PC surface and the particle boundaries are shown by black lines. One can see that the particle indeed perturbs the BSW field. First, there is a reflection which causes the interference pattern to the left of the particle. Second, refraction takes place which leads to the change of the BSW field distribution to the right of the particle. By using the momentum conservation law, one can deduce from the figure that the optically induced force is directed to the upper right.

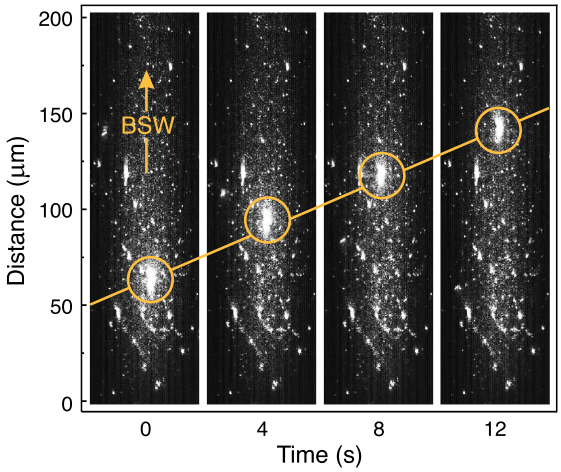

Fig. 3. Time-sequenced set of microimages of a particle at the PC surface. The bright area on the images corresponds to the BSW propagation region, and the large spots inside the circles correspond to the microparticle propelled by the BSW evanescent field.

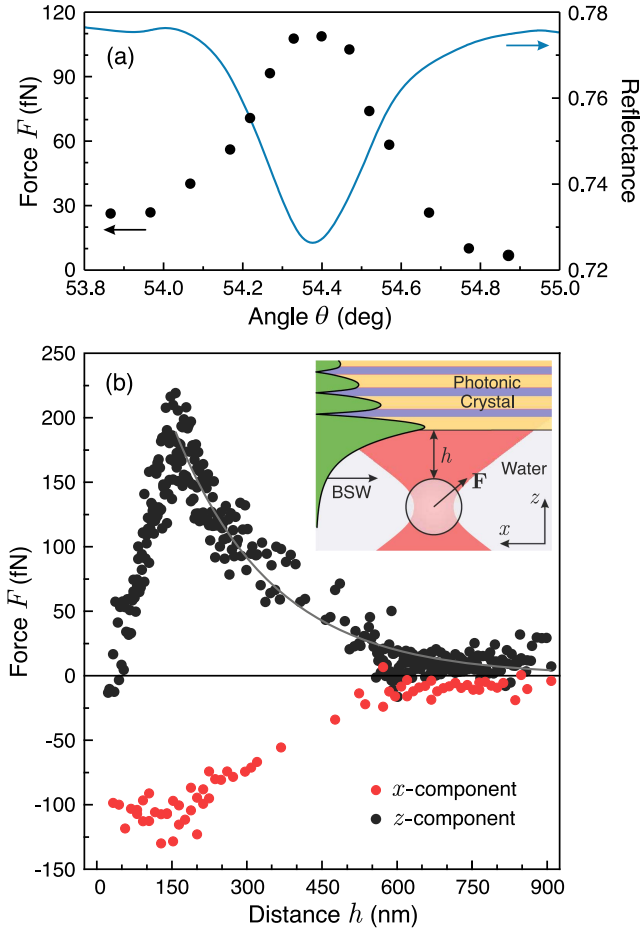

Fig. 4. (a) Experimental angular dependences of the PC reflectance (solid curve) and the magnitude of the BSW-generated force acting on a trapped microparticle at a PC/particle gap of approximately 300 nm (dots). Angle θ is the angle of incidence in the prism [see the inset in Fig. 2(a)]. The peak value corresponds to the BSW resonance angle. (b) x- (red dots) and z-coordinate (black dots) projection values of the BSW-generated force as a function of the distance between the trapped microparticle and the PC surface.

The simulation was carried out for different particle positions, and the results were used for the optical force calculation by integrating the Maxwell stress tensor. The dependence of the calculated optical force on the PC/particle gap is shown in Fig. 5(b). It is well fitted by an exponential function. Thereby, we suppose that the reason of the force diminution is connected to the presence of the surfactant in the sample which has not been taken into account at the simulation. One of the possible mechanisms is light-induced SDS redistribution.

The gradient force acting on a particle in the BSW field can be easily estimated in the dipole approximation by integrating the unperturbed energy density over the particle volume [39]. Because of the higher field enhancement at the resonance, the BSW-induced force can be expected to be considerably higher

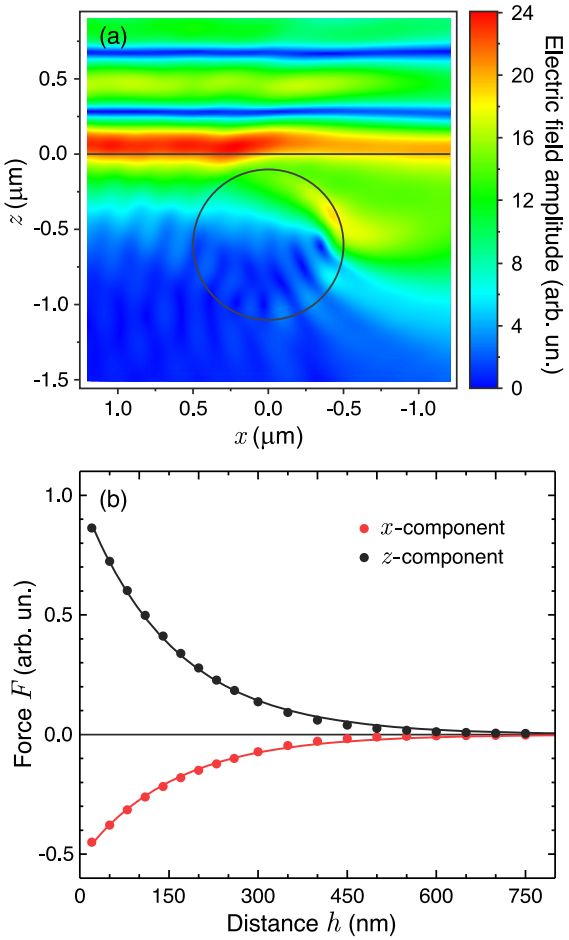

Fig. 5. (a) Calculated distribution of BSW electric field amplitude in the presence of a 1 μm particle at a PC/particle gap of 100 nm. (b) Calculated x- (red dots) and z-coordinate (black dots) projection values of the BSW-generated force as a function of the distance between the microparticle and the PC surface.

than the surface plasmon-induced force at the same exciting beam intensity. In fact, the angular divergence of the beam should be taken into account, and it is reasonable to calculate the optical force by the plane-wave expansion of the exciting radiation. Using our experimental conditions, the maximum BSW gradient force value of 150 fN, which is close to the maximum value of the measured force z-projection, can be obtained.

In conclusion, Bloch surface waves in 1D photonic crystals have been shown to be a promising tool for the optical manipulation of microparticles. The forces acting on a 1 μm polystyrene sphere in the BSW field have been measured using photonic force microscopy. Values of approximately 0.2 pN at an exciting beam intensity of 1.6 kW/cm^2 have been recorded, which are sufficient for particle localization near the PC surface and the propulsion of the particle in the direction of the BSW propagation.

Funding. Russian Foundation for Basic Research (RFBR) (simulations); Russian Science Foundation (RSF) (experiment) (15-02-00065).

REFERENCES

1. A. Ashkin, J. M. Dziedzic, J. E. Bjorkholm, and S. Chu, Opt. Lett. **11**, 288 (1986).
2. S. Hénon, G. Lenormand, A. Richert, and F. Gallet, Biophys. J. **76**, 1145 (1999).
3. C. Xie, M. A. Dinno, and Y.-Q. Li, Opt. Lett. **27**, 249 (2002).
4. E. V. Lyubin, M. D. Khokhlova, M. N. Skryabina, and A. A. Fedyanin, J. Biomed. Opt. **17**, 101510 (2012).
5. S. M. Block, L. S. B. Goldstein, and B. J. Schnapp, Nature **348**, 348 (1990).
6. T. Nishizaka, H. Miyata, H. Yoshikawa, S. Ishiwata, and K. Kinosita, Jr., Nature **377**, 251 (1995).
7. M. D. Wang, H. Yin, R. Landick, J. Gelles, and S. M. Block, Biophys. J. **72**, 1335 (1997).
8. J. C. Crocker and D. G. Grier, Phys. Rev. Lett. **73**, 352 (1994).
9. E. Schäffer, S. F. Nørrelykke, and J. Howard, Langmuir **23**, 3654 (2007).
10. M. N. Romodina, M. D. Khokhlova, E. V. Lyubin, and A. A. Fedyanin, Sci. Rep. **5**, 10491 (2015).
11. S. Lin, E. Schonbrun, and K. Crozier, Nano Lett. **10**, 2408 (2010).
12. Y.-F. Chen, X. Serey, R. Sarkar, P. Chen, and D. Erickson, Nano Lett. **12**, 1633 (2012).
13. N.-T. Huang, H.-l. Zhang, M.-T. Chung, J. H. Seo, and K. Kurabayashi, Lab Chip **14**, 1230 (2014).
14. D. Erickson, X. Serey, Y.-F. Chen, and S. Mandal, Lab Chip **11**, 995 (2011).
15. M. L. Juan, M. Righini, and R. Quidant, Nat. Photonics **5**, 349 (2011).
16. K. Wada, K. Sasaki, and H. Masuhara, Appl. Phys. Lett. **76**, 2815 (2000).
17. G. Volpe, R. Quidant, G. Badenes, and D. Petrov, Phys. Rev. Lett. **96**, 238101 (2006).
18. B. S. Schmidt, A. H. J. Yang, D. Erickson, and M. Lipson, Opt. Express **15**, 14322 (2007).
19. M. Righini, G. Volpe, C. Girard, D. Petrov, and R. Quidant, Phys. Rev. Lett. **100**, 186804 (2008).
20. A. N. Grigorenko, N. W. Roberts, M. R. Dickinson, and Y. Zhang, Nat. Photonics **2**, 365 (2008).
21. K. Wang, E. Schonbrun, P. Steinvurzel, and K. B. Crozier, Nano Lett. **10**, 3506 (2010).
22. P. Yeh, A. Yariv, and A. Y. Cho, Appl. Phys. Lett. **32**, 104 (1978).
23. W. M. Robertson and M. S. May, Appl. Phys. Lett. **74**, 1800 (1999).
24. F. Villa, L. E. Regalado, F. Ramos-Mendieta, J. Gaspar-Armenta, and T. Lopez-Ríos, Opt. Lett. **27**, 646 (2002).
25. E. Descrovi, F. Frascella, B. Sciacca, F. Geobaldo, L. Dominici, and F. Michelotti, Appl. Phys. Lett. **91**, 241109 (2007).
26. Y. Li, T. Yang, S. Song, Z. Pang, G. Du, and S. Han, Appl. Phys. Lett. **103**, 041116 (2013).
27. T. Sfez, E. Descrovi, L. Yu, M. Quaglio, L. Dominici, W. Nakagawa, F. Michelotti, F. Giorgis, and H. P. Herzig, Appl. Phys. Lett. **96**, 151101 (2010).
28. L. Yu, E. Barakat, T. Sfez, L. Hvozdara, J. Di Francesco, and H. P. Herzig, Light Sci. Appl. **3**, e124 (2014).
29. E. Descrovi, T. Sfez, M. Quaglio, D. Brunazzo, L. Dominici, F. Michelotti, H. P. Herzig, O. J. F. Martin, and F. Giorgis, Nano Lett. **10**, 2087 (2010).
30. I. V. Soboleva, V. V. Moskalenko, and A. A. Fedyanin, Phys. Rev. Lett. **108**, 123901 (2012).
31. L. P. Ghislain and W. W. Webb, Opt. Lett. **18**, 1678 (1993).
32. E.-L. Florin, A. Pralle, J. K. H. Hörber, and E. H. K. Stelzer, J. Struct. Biol. **119**, 202 (1997).
33. R. M. Simmons, J. T. Finer, S. Chu, and J. A. Spudich, Biophys. J. **70**, 1813 (1996).
34. K. Berg-Sørensen and H. Flyvbjerg, Rev. Sci. Instrum. **75**, 594 (2004).
35. K. C. Neuman and S. M. Block, Rev. Sci. Instrum. **75**, 2787 (2004).
36. P. Jákl, M. Šerý, J. Ježek, A. Jonáš, M. Liška, and P. Zemánek, J. Mod. Opt. **50**, 1615 (2003).
37. D. A. Shilkin, E. V. Lyubin, I. V. Soboleva, and A. A. Fedyanin, J. Exp. Theor. Phys. Lett. **98**, 644 (2014).
38. A. Banerjee and K. D. Kihm, Phys. Rev. E **72**, 042101 (2005).
39. T. Tlusty, A. Meller, and R. Bar-Ziv, Phys. Rev. Lett. **81**, 1738 (1998).